This document is the submitted manuscript version of a published article that appeared in its final form in the International Journal of Pharmaceutics, copyright ELSEVIER. To access the final edited and published work see: **https://doi.org/10.1016/j.ijpharm.2021.120464**

Microfluidics for nanomedicines manufacturing: an affordable and low-cost 3D printing approach

Mattia Tiboni[1], Massimiliano Tiboni[2], Alessio Pierro[3], Marco del Papa[3], Simone Sparaventi[3], Marco Cespi[4] and Luca Casettari[1*]

[1]*Department of Biomolecular Sciences, University of Urbino Carlo Bo, Piazza del Rinascimento, 6, 61029 Urbino (PU), Italy.*

[2]*R&D department, Idrofoglia s.r.l., Via Provinciale, 14, 61026 Lunano (PU), Italy*

[3]*R&D department, TechFem s.p.a., Via G. Toniolo, 1/d, 61032 Fano (PU), Italy*

[4]*School of Pharmacy, University of Camerino, 62032 Camerino (MC), Italy*

ABSTRACT

During the last decade, an innovative lab on a chip technology known as microfluidics became popular in the pharmaceutical field to produce nanomedicines in a scalable way. Nevertheless, the predominant barriers for new microfluidics users are access to expensive equipment and device fabrication expertise.

3D printing technology promises to be an enabling new field that helps to overcome these drawbacks expanding the realm of microfluidics. Among 3D printing techniques, fused deposition modeling allows the production of devices with relatively inexpensive materials and printers.

In this work, we developed two different microfluidic chips designed to obtain a passive micromixing by a "zigzag" bas-relief and by the presence of "split and recombine" channels. Computational fluid dynamic studies improved the evaluation of the mixing potential. A fused deposition modeling 3D printer was used to print the developed devices with polypropylene as manufacturing material. Then, two different model nanocarriers (*i.e.*, polymeric nanoparticles and liposomes), loading cannabidiol as model drug, were formulated evaluating the influence of manufacturing parameters on the final nanocarrier characteristics with a design of experiments approach (2-level full factorial design).

Both the chips showed an effective production of nanocarriers with controllable characteristics and with a good loading degree.

These polypropylene-based microfluidic chips could represent an affordable and low-cost alternative to common microfluidic devices for the effective manufacturing of nanomedicines (both polymer- and lipid-based) after appropriate tuning of manufacturing parameters.

Keywords: FDM; nanomedicine; polymeric NPs; liposomes; cannabidiol; drug delivery systems, CFD.

1. INTRODUCTION

The scale up of nanocarriers manufacturing is one of the main issues for the translation from the bench to the clinic of innovative drug delivery nanosystems (DDS) (Metselaar and Lammers, 2020). Common methods such as thin layer evaporation or nanoprecipitation involve several steps and usually lack of reproducibility, controllability, and low production rate (Valencia et al., 2012). In a typical colloidal system production, the procedure is based on a bottom-up approach, where most of the theoretical works describing the formation process are based on the classical nucleation theory (Liu et al., 2019; Mer, 1952).

During the last few years, the concept of "lab on a chip" became popular among researchers facilitating the development of more precise systems for healthcare applications by the miniaturization of conventional processes (Daw and Finkelstein, 2006; Wu et al., 2020). Among different lab on a chip technologies, microfluidics became an innovative manufacturing approach in the pharmaceutical and biomedical fields by manipulating nanoliters scale of fluids in submillimeter channels. It allows to effectively control the final formulation characteristics by tuning the manufacturing parameters (Martins et al., 2018).

Even if the microfluidic method is not a new story, the colloidal DDS-assisted production has drawn increased interest due to several advantages such as high reproducibility, low batch-to-batch variation, better control over particle characteristics, and ease to scale-up (Zhao et al., 2020). Moreover, microfluidics can sharply increase the surface area-to-volume ratio by several orders of magnitude allowing a more efficient mass and heat transfer within the system (Capretto et al., 2011). The production of nanocarriers within this technique needs mixing of fluids in sub-millimeter channels that become difficult into simple smooth microchannels where the flow remains laminar. To overcome this problem different micromixers have been developed and classified as active and passive micromixers (Hessel et al., 2005). Active micromixers take advantage of external sources of energy such as electric or magnetic fields and acoustic waves. Even if the mixing is rapid within these devices, they are more difficult to fabricate, integrate, and operate compared to passive micromixers. Passive micromixers are based on shape modification of the structure of microchannels to produce a specific flow pattern that enhances mixing such as the presence of obstacle, bas-reliefs, or split and recombine microchannels that induce whirl flow and recirculation creating transversal mass transport (Lee et al., 2016).

Common microfluidic device fabrication protocols include photolithography and micromachining. The predominant barriers for new users and alternative applications are access to expensive equipment and device fabrication expertise.

3D printing technology promises to be an enabling new field that reduces complexity and costs and thus expands the realm of microfluidics (Pranzo et al., 2018). Among the 3D printing techniques currently available, fused deposition modeling (FDM) utilizes a heated nozzle to extrude a thermoplastic polymeric filament layer over layer to form the desired 3D object (Melocchi et al., 2020). This approach presents several advantages including relatively inexpensive materials and printers, low maintenance costs, a large selection of commercially available materials, the ease of initial use and the ability to start, stop, and integrate complexity on the fly (Romanov et al., 2018). Compared to expensive microfluidic chip production techniques, 3D printing enables a reduction in the resources and skills required to manufacture microfluidic devices, micromixer included as already reported in the literature (Morgan et al., 2016; Tothill et al., 2017; Vasilescu et al., 2020; Waheed et al., 2016).

In this work, we developed two different 3D printed microfluidic chips using polypropylene (PP) in an FDM 3D printer. The two chips rely on passive micromixing due to the presence of a "zigzag bas-relief" and a "split and recombine" channel shape, respectively. PP was selected as the manufacturing material because it is a robust, flexible, and chemically inert polymer, resistant to the majority of organic solvents such as acetone, acetonitrile, ethanol, and methanol. (Price et al., 2020).

The microfluidic designs were first characterized by computational fluid dynamics (CFD) studies and then printed to be evaluated for the manufacturing of nanocarriers.

Both lipid-based and polymer-based nanocarriers were produced and characterized, encapsulating cannabidiol (CBD) as a model active molecule since it has shown different therapeutic effects such as anti-inflammatory, pain-relieving, antioxidant, immunomodulatory, antidepressant, antiepileptic, anticonvulsant and, antineoplastic effects (Pagano et al., 2020). The influence of manufacturing parameters was evaluated with a design of experiment (DoE) approach.

2. MATERIALS AND METHODS

2.1 Materials

Neutral polypropylene 3D printing filament was kindly gifted from Verbatim (Italy), Phospholipon 90-G (SPC, soybean lecithin, 94 % of phosphatidylcholine) was kindly provided by Lipoid (Germany), cholesterol was kindly provided by Croda (United Kingdom), poly(lactic-co-glycolic acid) (PLGA Purasorb® 5002A) was kindly provided by Corbion (The Netherlands). Cannabidiol (CBD) was purchased from VerusHemp (United Kingdom). All the other solvents used were HPLC grade.

2.2 Design of microfluidic chips

The original 3D projects were designed using the computer aided design (CAD) software SolidWorks 2018 (Dassault Systèmes, France). The two designs were developed to have an effective passive micromixing with "zigzag" bas-relief and "split and recombine" channels. The files were exported from the CAD software as STL (Stereolithography interface format) to be then converted in machine language with a computer aided manufacturing (CAM) software (STL file provided as supplementary material).

2.3 Computational fluid dynamics studies

The single-field incompressible Navier–Stokes equations modeled with the volume-of-fluid (VOF) method was used for the CFD simulations of two-phase flow (Hirt and Nichols, 1981). The VOF model is a surface-tracking technique that uses a fixed mesh system to solve geometry interfaces and interactions between different fluids. The fluid dynamics of two-phase flows are described with a set of single-field equations which are obtained through conditional volume averaging of the local instantaneous conservation equations of mass and momentum.

The indicator function (α) allows obtaining the location of the interface, which is equal to the volume fraction of a phase in each cell. The solution of the continuity equation (1) for the volume fraction (α) of one of the phases enables to track the evolution of the interphase surface (Hirt and Nichols, 1981).

$$\frac{\partial \alpha}{\partial t} + \nabla \cdot (\alpha U) = 0 \qquad (1)$$

where α is the volume fraction and U is the velocity field. Since α is discontinuous at the phase boundaries, and it is important to have this discontinuity sharp enough to precisely capture the interface between two phases, an additional term has been introduced, which is a function of the relative velocity between two phases U_r, as in equation (2).

$$\frac{\partial \alpha}{\partial t} + \nabla \cdot (\alpha U) + \nabla \cdot (\alpha(1-\alpha)U_r) = 0 \qquad (2)$$

It is worth noticing that the equation is exact because no assumptions are employed in its derivation. In the VOF method, only the single continuity and momentum equations are solved for the entire domain. This approach is known as the "one-fluid" approach (Gueyffier et al., 1999). Therefore, the variables and material properties are defined as volume averaged of the two phases in each cell, as shown in equations (3) and (4)

$$\rho = \alpha\rho_1 + (1-\alpha)_{\rho_2} \quad (3)$$

$$\mu = \alpha\mu_1 + (1-\alpha)_{\mu_2} \quad (4)$$

The governing equations were solved with the finite-volume-based, open-source CFD toolbox, OpenFOAM (OpenCFD Ltd) (Desir et al., 2020; Weller et al., 1998). The dispersed phase, water, flows into the micromixer from one inlet, while the continuous organic phase, e.g., Acetonitrile and ethanol, flows into the chip from the other inlet and mixes with the water. At the inlet, a zero-pressure gradient and constant velocity were used as boundary conditions. At the outlet, the velocity and volume fraction were set to be zero-gradient, and the pressure to be atmospheric.

2.4 3D printing of polypropylene microfluidic chips

3D-printed PP microfluidic chips were produced via fused deposition modeling (FDM) using an Ultimaker 3 printer (Ultimaker, The Netherlands). Both the developed devices were printed at a print speed of 25 mm/s with a nozzle temperature of 205 °C. The infill density was set at 100 % and the build plate was preheated at 85 °C after the application of a polypropylene adhesion sheet (Ultimaker, The Netherland). The original STL file was converted to a print pattern using Ultimaker Cura 4.6.1 software (Ultimaker, The Netherlands). Alternating 50 μm thick layers were printed such that the pattern ran parallel to the length of the device, enabling leak-free and semi-transparent devices to be printed with PP. Probe needles were used to connect the chip with pump tubing. The effective dimensions of the microfluidic channels were evaluated using a digital microscope and then, a colored aqueous solution was run through the microchannels to confirm that the fluids were free to flow through the chips.

2.5 Microfluidic formulation of polymeric nanoparticles

For the preparation of PLGA NPs by microfluidics, the 3D printed chip was connected to two syringes mounted on two syringe pumps (Aladdin syringe pump, WPI Europe, Germany) through polyethylene tubing. A precise amount of PLGA alone or PLGA and CBD dissolved in acetonitrile was pumped against water at controlled flow rates and the samples were collected from the outlet of the chip. Two different final polymer concentrations were evaluated, *i.e.*, 5 and 10 mg/mL. The flow rate ratios (FRR) evaluated were 1:3 and 1:1 (ACN:water) and the total flow rates (TFR) were 10 and 12 mL/min. The amount of CBD added was 3 % w/w (Loading degree max 3%). The organic solvent was evaporated under a stream of nitrogen (Trotta et al., 2002). The specific

experimental conditions used for the preparation of all NPs were defined according to the DoE reported in the method section 2.7.

2.6 Microfluidic formulation of liposomes

For the preparation of liposomes by microfluidics, the 3D printed chip was connected to two syringes mounted on syringe pumps (Aladdin syringe pump, WPI Europe, Germany) through polyethylene tubing. A precise amount of SPC and cholesterol (3:1 w/w) or SPC, cholesterol, and CBD dissolved in ethanol was pumped against water at controlled flow rates, and the samples were collected from the outlet of the chip. Two different final lipids concentrations were evaluated, *i.e.*, 10 and 15 mg/mL. The FRR evaluated were 1:3 and 1:5 (ethanol:water) and the TFR were 10 and 12 mL/min. The amount of CBD added was 3 % w/w (Loading degree max 3%). The organic solvent was evaporated under a stream of nitrogen (Trotta et al., 2002). The specific experimental conditions used for the preparation of all liposomes were defined according to the DoE reported in the method section 2.7.

2.7 Design of the experiments (DoE)

The effect of chip design and the preparation conditions (polymer/lipids concentration, FRR, and TFR) on NPs/liposomes size and polydispersity were evaluated by applying 2 levels full factorial design, characterized by 2^f experiments (where 2 is the number of levels and f is the number of factors) as reported in table 1.

Table 1. Two levels full factorial design matrix for the evaluation of the effect of chip design and preparation conditions.

RUN	CHIP	CONCENTRATION	TFR	FRR
1	Z	-1	-1	-1
2	C	-1	-1	-1
3	Z	+1	-1	-1
4	C	+1	-1	-1
5	Z	-1	+1	-1
6	C	-1	+1	-1
7	Z	+1	+1	-1
8	C	+1	+1	-1
9	Z	-1	-1	+1
10	C	-1	-1	+1

11	Z	+1	-1	+1
12	C	+1	-1	+1
13	Z	-1	+1	+1
14	C	-1	+1	+1
15	Z	+1	+1	+1
16	C	+1	+1	+1

The design is characterized by a categorical factor, the chip design coded as Z (zigzag bas-relief) or C (split and recombine channels), and by three numerical factors, concentration, TFR, and FRR coded as -1 and +1. The numerical values of the coded variables are reported in table 2. The two nanocarriers were prepared by varying all the parameters within the same range with the only exception for the FRR. In this case, a larger range was selected since for values higher than 1:3 the preparation of the polymeric nanoparticles was not possible due to the precipitation of the polymer and chip clogging.

Table 2. Manufacturing condition and their corresponding numerical values of the coded variable.

Coded Variable	NPs			Liposomes		
	Concentration	**TFR**	**FRR***	**Concentration**	**TFR**	**FRR***
-1	5 mg/ml	10 ml/min	0.33	5 mg/ml	10 ml/min	0.2
+1	10 mg/ml	12 ml/min	1	10 mg/ml	12 ml/min	0.33

* The FRR values used in the DoE represents the volumetric ratio of the organic and aqueous phases mixed through the microfluidic chip. Thus, the values of 0.2, 0.33, and 1 were used to numerically describe the FRR 1:5, 1:3, and 1:1 respectively.

All the NPs and liposomes prepared according to the DoE were characterized in terms of average particle size and polydispersity index as described in section 2.8. These two parameters represent the responses of the designs.

For each response, the two design were analysed by multilinear regression using a first order model:

$$y = \beta_0 + \sum_{i=1}^{n} \beta_i \cdot x_i + \sum_{i<j}^{n} \beta_{ij} \cdot x_i x_j$$

Where y is the response, β_0 is the model constant, β_i is the coefficient corresponding to the variables x_i (linear terms), and β_{ij} are the coefficients associated with the variables $x_i x_j$ (first-order interaction terms).

The goodness of fitting was evaluated through the adjusted coefficient of multiple determination (R^2_{adj}), while the residues analysis was used to test if the models meet the assumptions of the analysis. The ANOVA and coefficient analysis were instead used to identify the relative magnitude and the statistical significance of all the model terms.

The DoE design and analysis was carried out with the Minitab 18 statistical software (2017 Minitab, Inc.).

2.8 Nanocarriers physicochemical characterization: DLS, AFM, DSC, LD%

Prepared formulations were characterized for their average particle size (Z-average) and polydispersity index (PDI) by dynamic light scattering (DLS) using a Malvern Zetasizer Nano S instrument (Malvern Instruments Ltd, UK). Moreover, the morphology of the nanocarriers was evaluated by atomic force microscopy (AFM). For the preparation of AFM surfaces, a drop of the nanocarrier suspension was deposed for 10 minutes on freshly cleaved mica surfaces, 0.5 x 0.5 cm in size. Then, the surfaces were washed, dried, and observed with the XE-100 Atomic Force Microscope (AFM, PARK System Inc., Suwon, South Korea). The employed probe was a μMasch 36C with a nominal constant force of 0.6 Nm. Scanning frequency was between 0.5 and 2 Hz. The instrument was set in true non-contact mode, with X–Y stage in a closed loop, while the Zscanner was set in closed loop and high voltage mode. The images were analyzed by XEI software (PARK Systems Inc., Suwon, South Korea).

Differential scanning calorimetry (DSC) studies were performed using a DSC 6000 (PerkinElmer, Norwalk, USA), equipped with an intracooler (Intracooler 2, PerkinElmer, Norwalk, USA) in an inert nitrogen atmosphere. CBD, PLGA and cholesterol were analyzed as powders meanwhile liposomes and NPs were analyzed as liquid dispersions. A small amount (2-4 mg for the powders, 4 mg for the liquid dispersions) of the samples was placed in an aluminum pan and analyzed, using an equal empty pan as reference. The liquid samples were analyzed from 10 °C to 80 °C at 10 °C/min meanwhile the solid samples were analyzed from 10 °C to 200 °C at 10°C/min. All runs were performed at least in triplicate.

The loading degree (LD%) was evaluated with a direct ultracentrifugation method. Briefly, a precise amount of nanocarriers was ultracentrifuged at 70000G for 1 hour and then the pellet was dissolved with acetonitrile. The obtained solution was analyzed by HPLC to evaluate the content of CBD. The LD% was calculated by the amount of total entrapped drug divided by the total nanocarrier weight.

2.9 HPLC method for the analysis of CBD

The content of CBD was assessed by high-performance liquid chromatography (HPLC Agilent 1260 Infinity II, Agilent, USA) using an isocratic mixture of 0.5 % formic acid in water and 0.5 % formic acid in acetonitrile (ratio 15:85) as mobile phase, with a flow rate of 1 mL/min in an

Agilent Poroshell 120 EC-C18, 100x4.6 mm, 2.7 μm column (Agilent, USA). The injection volume was 20 μL and the detection signal was recorded at 220 nm keeping the analysis system at room temperature.

2.10 Statistics

The data presented are the mean ± standard deviation of triplicate measurements and are representative of at least three independent experiments.

3. RESULTS AND DISCUSSION

3.1. Microfluidic chips development

The development of a 3D printed object starts from the computer assisted design (CAD) of the model. Microfluid chips can be engineered with active or passive micromixing depending on the characteristics needed. Active micromixing requests a higher complexity and the presence of an external source of energy such as ultrasounds or magnetic fields. On the contrary, passive micromixing does not need any external energy source because it takes advantage of the presence of perturbations in the microchannels such as bas-relief, splits, 3D structures that induct a chaotic advection effect. These modifications in the microfluidic channels help to increase the contact surface and contact time between the species by splitting, stretching, folding, and breaking the flows (Capretto et al., 2011; Hessel et al., 2005; Lee et al., 2016).

In this work, we developed two different micromixing designs with a "zigzag 3D structure" and a "split and recombine circular sub-channels". These two designs were chosen taking inspiration from literature in which different microchannel shapes have been analyzed to evaluate the micromixing potential. The "zigzag structure" takes advantage of the presence of bas-reliefs similar to the most common herringbone structure meanwhile the "split and recombine" structure helps the mixing by splitting the flow also with a change in microchannel section that create unbalanced collisions of the fluid streams where the microchannels recombine together. The circular structure was selected over a rhombic one since it resulted in a higher mixing performance (Ansari and Kim, 2010).

The FDM printing technique was selected since it presents several advantages such as a large selection of relatively inexpensive materials and printers, low maintenance costs and the ease of initial use. It is worth to note that even if another printing technique utilized to produce microfluidic systems named stereolithography (SLA) could bring to higher accuracy and surface definition, it requires the utilization of only photopolymerizing resins as manufacturing material. Most of the literature on 3D

printed microfluidics use their own 3D printed setup or develop their own resin, optimized for the selected printer. This can result in difficulties when trying to replicate their work, limiting the knowledge transfer potential (Heidt et al., 2020). In this work, using FDM we have had the possibility to choose, among many different materials, PP as printing material and take the advantage of its properties such as robustness, flexibility, and chemical resistance to organic solvents.

Figure 1A represents the 3D design of the zigzag chip (Z chip) which has two inlets that are combined with a T-junction into the main channel. The main channel presents the zigzag 3D structure along all its length to induce the desired chaotic mixing. The channels of this chip present a square section with a section of 1 mm while the zigzag structure has a height of 500 µm. The total length of the main channel is 60 mm.

Figure 1B represents the second microfluidic design which takes advantage of split and recombine sub-channels (C chip). Also, in this case, it presents two squared inlets (1 mm side) combined with a T-junction into the main channel. The subsequent circular splitting is repeated six times and kept unequal to have a difference in the velocity of the fluids and therefore unbalanced collisions of the fluid streams (Ansari and Kim, 2010). The major sub-channel has a section of 600 µm while the minor sub-channel has a section of 400 µm both squared.

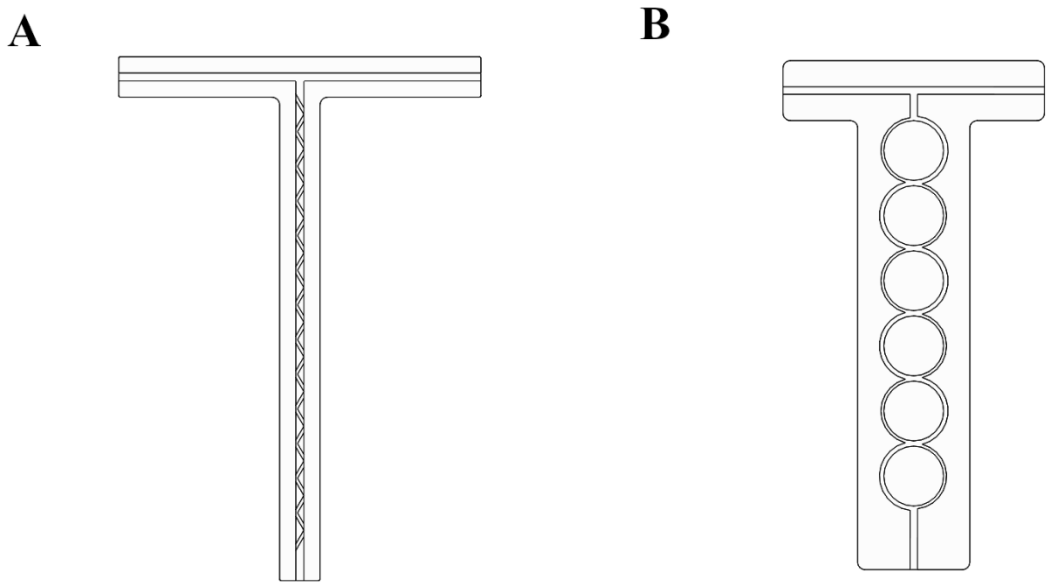

Figure 1. Computer aided design models of A) "Z" (zigzag design) microfluidic chip and B) "C" (Split and recombine design) microfluidic chip.

These two models were evaluated with computational fluid dynamic (CFD) studies to assess the effective micromixing potentiality. This studies also help us to confirm that the final dimensions of the chips were sufficient to reach a complete mixing. Acetonitrile and ethanol were selected as the

organic phase against water in the two inlets of each microfluidic chip. These two solvents were selected to produce PLGA NPs and liposomes, respectively. The inlets and outlet have been assigned uniform velocity profile and zero static pressure as boundary conditions. The density of water, ethanol, and acetonitrile are 9.97 x 10^2, 7.89 x 10^2, and 7.86 x 10^2 kg/m^3, respectively. FRR 1:3 and 1:1 were evaluated for ACN:water (PLGA NPs) meanwhile FRR 1:3 and 1:5 were evaluated for ethanol:water (Liposomes).

Figure 2 shows the distribution of the volumetric fraction of each solvent (ACN:water) with an RGB scale that represent the water fraction.

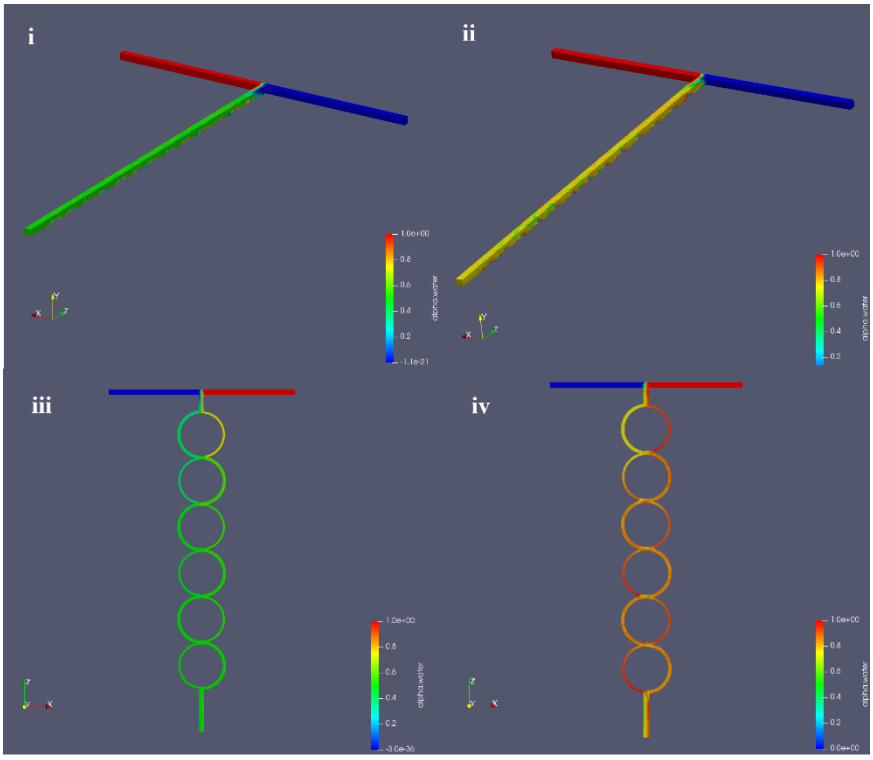

Figure 2. Computational fluid dynamic simulation of Z and C chips with water and ACN. The distribution of the volumetric fraction of each solvent is represented with an RGB scale. i) and ii) show Z chip at FRR 1:1 and 1:3, respectively. iii) and iv) show C chip at FRR 1:1 and 1:3, respectively. The red color is for water and blue color is for ACN.

These results demonstrate that the developed microfluidic chips present an effective mixing performance. In particular, the mixing was more effective at FRR 1:1 (Figure 2i, iii) for both chips reaching a complete mixing after 0.79 sec in the Z chip (Figure 2i) and after 1 sec and 3 circular sub-channels in the C chip (Figure 2iii). At FRR 1:3 (Figure 2ii, iv), the mixing performance was lower reaching a complete mixing only at the end of the microfluidic chip (1.97 sec in the Z chip and 1.6 sec in the C chip). FRR 1:5 results are not shown since this parameter brought to chip occlusion due to polymer precipitation during the manufacturing of the NPs.

Figure 3 shows the distribution of the volumetric fraction of each solvent (ethanol:water) with an RGB scale that represent the water fraction.

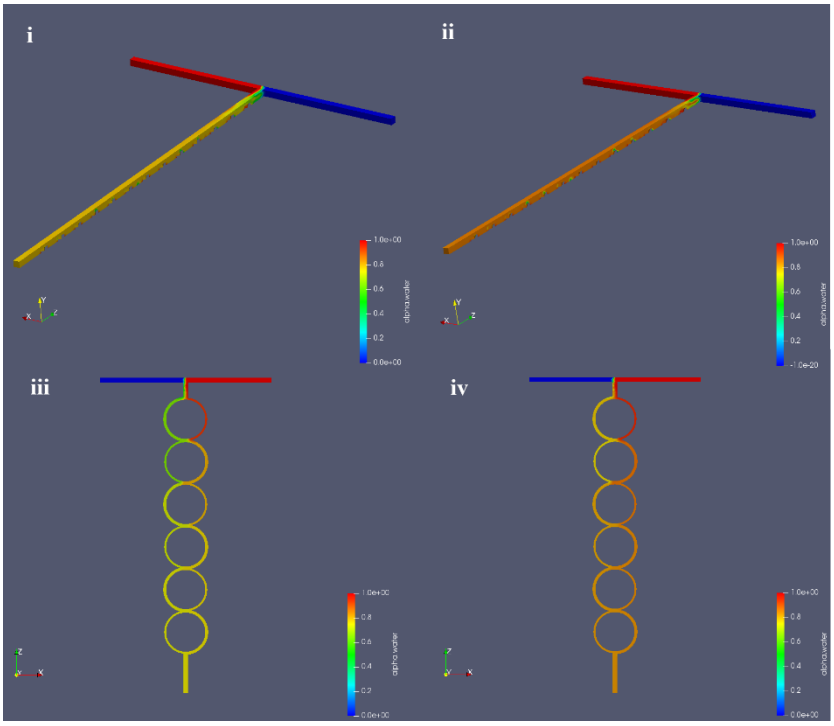

Figure 3. Computational fluid dynamic simulation of Z and C chips with water and ethanol. The distribution of the volumetric fraction of each solvent is represented with an RGB scale. i) and ii) show Z chip at FRR 1:3 and 1:5, respectively. iii) and iv) show C chip at FRR 1:3 and 1:5, respectively. The red color is for water and blue color is for ethanol.

Even in this case, the mixing performance was effective at both the FRR evaluated (1:3 and 1:5) confirming a potential to produce lipidic nanocarriers. The complete mixing of the two fluids was reached with all the conditions studied in less than 1.9 sec (Figure 3i 1.41 sec, ii 1.87 sec, iii 1.49 sec, iv 1.49 sec).

According to these results, the two chips were printed using polypropylene as printing material. This polymer was selected because of its chemical resistance to commonly used microfluidic solvents such as ACN, ethanol, acetone, and methanol (Price et al., 2020) compared to the polylactic acid (PLA) commonly used to print objects with the FDM technique. During the manufacturing of the chips, the effective channel dimensions were evaluated with a digital microscope (Figure 4A Z chip, Figure 4B C chip) showing an accordance with the dimension of the CAD project and thus confirming the optimal printing resolution. After the manufacturing of the two chips, a colored aqueous solution was run through the microchannels to confirm that the fluids were free to flow through the chip (Figure 4C, D).

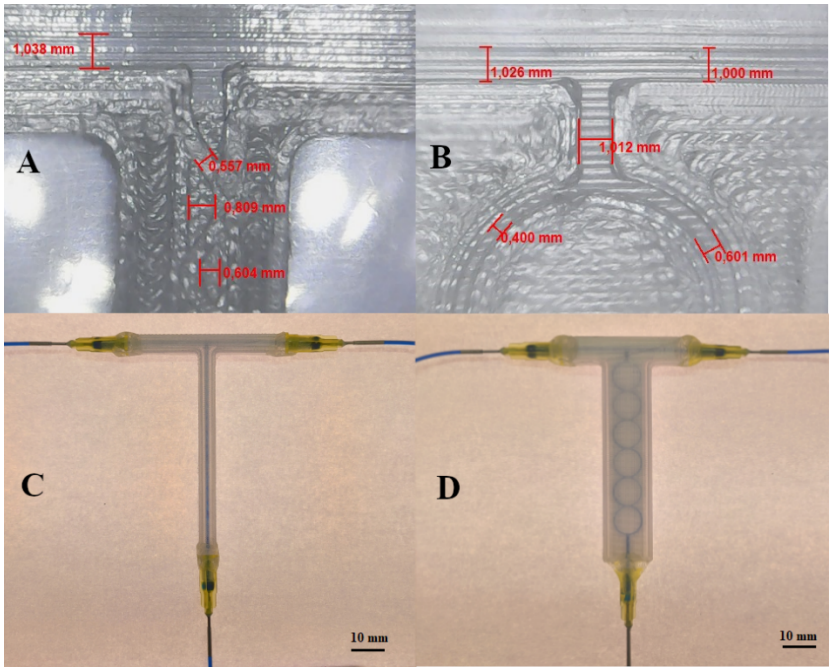

Figure 4. Printed channels measure of Z chip (A) and C chip (B). In the Z chip it can be observed the zigzag structure meanwhile in the C chip it is notable the asymmetric dimensions of the splitted channels. C and D show a colored aqueous solution running through the two printed chips.

3.2 Nanocarriers manufacturing and evaluation of the influence of microfluidic parameters

The two 3D-printed microfluidic chips were utilized to produce both polymeric and lipidic nanocarriers. PLGA and SPC/cholesterol were selected as model excipients as they have been already widely utilized in the production of polymeric NPs and liposomes, respectively.

To evaluate as the different microfluidic parameters and the chip design affect the two types of prepared nanocarriers it has been decided to perform a factor influence study applying a 2-level factorial design (Lewis et al., 1998). Once all the experimental runs provided by the DoE (table 1) were carried out and the samples characterized, it has been performed a preliminary assessment of the obtained data plotting them in an individual value plot (Figure 5). Interestingly, NPs and liposomes appear completely different, with the first showing a much wider size and polydispersity distributions with a higher median value for the size compared with the latter.

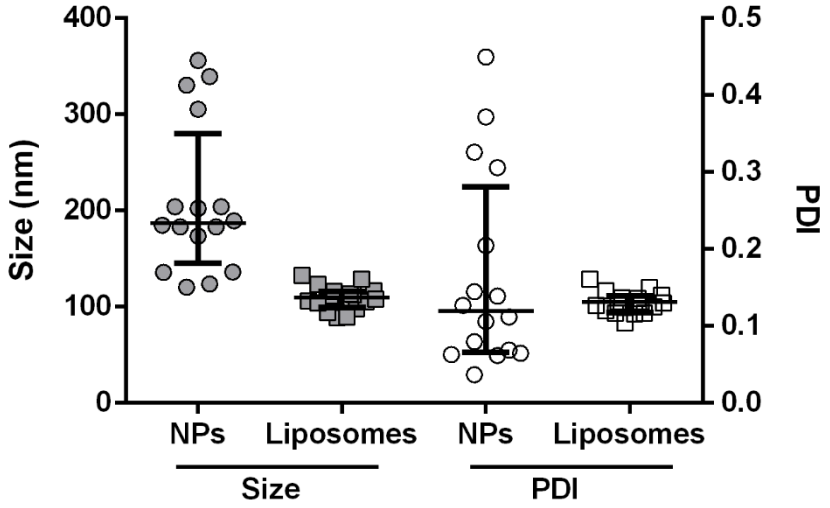

Figure 5. Individual value plot of z-average diameter and PDI. The lines above each group represent the median (central line) and the interquartile range (distance between the two outer lines).

Such results could be intrinsic to the two nanocarriers but could also be due to the FRR, which for practical reasons (Polymer precipitation and consequent chip occlusion with FRR 1:5), is the only preparation variable applied in different range for NPs and liposomes (from 1:1 to 1:3 and from 1:3 to 1:5 for NPs and liposomes. respectively). To verify this hypothesis, the size and PDI of NPs and liposomes prepared at the same FRR (1:3) were compared with the t-test. The results indicate statistically significant differences and consequently the differences observed in figure 5 cannot be attributed to the different FRR range used (Supplementary figure 1). Another preliminary evaluation concerns the check of any correlation between the two responses (size and PDI) for each nanocarrier. Pearson correlation analysis has been performed and the results, once again, are specific for NPs and liposomes (Supplementary figure 2). In fact, while for liposomes no correlation was observed, for NPs size and PDI show a strong positive correlation (Pearson coefficient equal to 0.932 with a P-value lower than 0.001).

The size and PDI values were then analyzed through multilinear regression to assess the influence of all the experimental variables. The results of DoE analysis (Considering the type of chip, excipient concentration, TFR and FRR as variables) are summarized using Pareto plots and "main effect" and "interaction" plots (Antoy, 2014) while all the detailed results, goodness of fit statistic, residual analysis, ANOVA, and coefficient analysis are reported in the supplementary material. The fitting procedure of PDI values for liposomes resulted to be poor (R^2_{adj} lower than 0.2 and non-significant model regression), suggesting as such a value are not influenced by the four-variable studied or the mathematical model is not adequate. For this reason, the PDI of liposomes will not be more discussed subsequently. The Pareto plots reported in figure 6 show which variables have a statistically

significant effect on the NPs and liposomes features. Interestingly, NPs and liposomes show different behaviour concerning the role of the preparation parameters. In fact, even if the polymer and lipid concentrations represent a crucial parameter for the preparation of both nanocarriers, the size of liposomes depends also on the chip design while that of the NPs are strongly affected by the FRR and the interaction between FRR and concentration. Another noteworthy aspect concerns the fact that the TFR does not exert any effect both on NPs and liposomes, at least within the range analysed. Moreover, the Pareto plots as well as the Anova and coefficient analysis reported in the supplementary materials demonstrate as the results for the size and PDI of NPs are equivalent, confirming that these two parameters are strongly correlated.

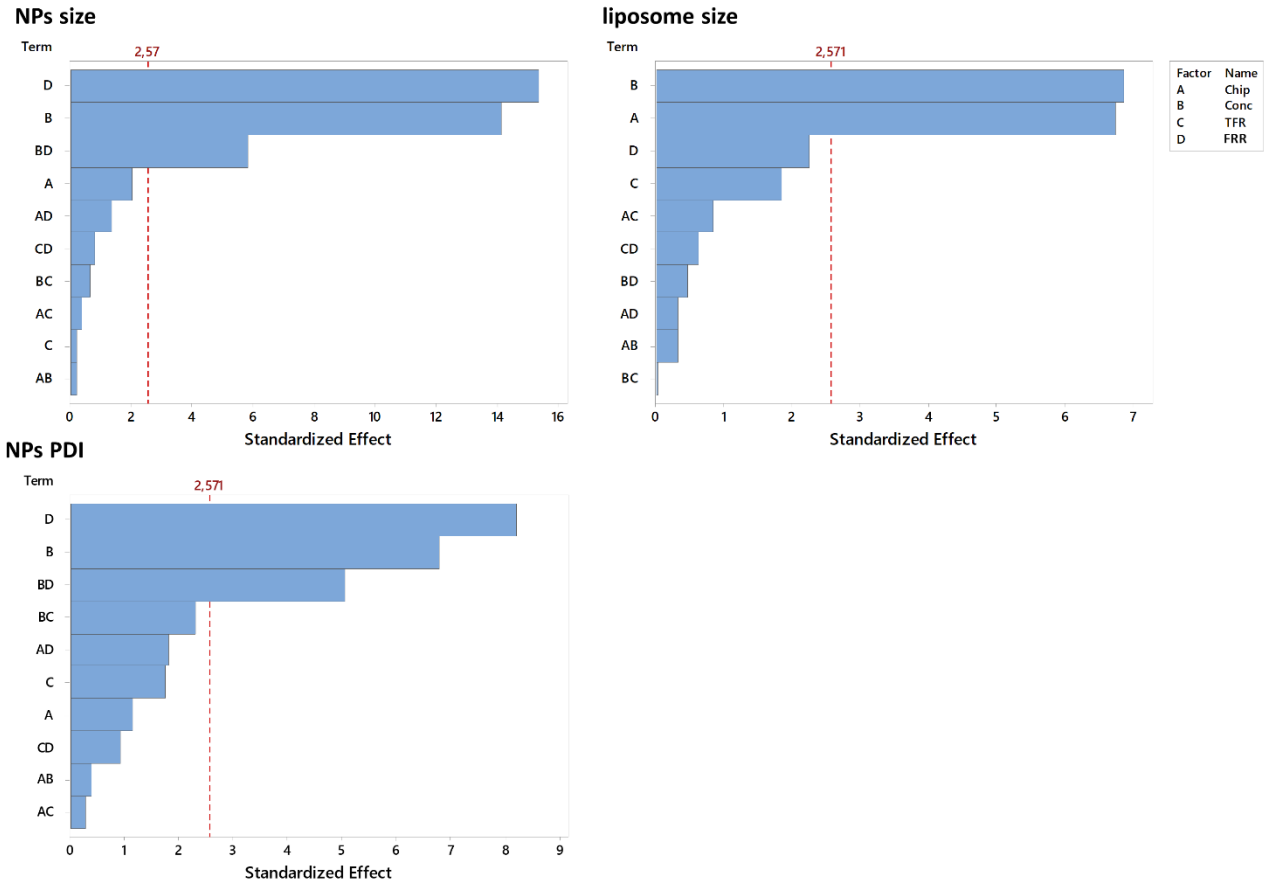

Figure 6. Pareto plots for the size of the NPs (Upper left panel), for the PDI of the NPs (lower left panel), and for the size of liposomes (upper right panel). The red line represents the statistically significance limit (the t-values corresponding at a one-sided probability of 0.025 from a t distribution with the same degree of freedom of the error term) when the relevance of a variable is reported as standardized effect (t-value of the coefficient).

The Pareto plots show the relevance of the investigated factors and their significance; however, the use of the "main effect" and "interaction" plots provides a more detailed picture of how significant factors influence responses (Antoy, 2014). The main effects and interaction plots in figure 7 refer

only to the factors that resulted statistically significant from the Anova and coefficient analyses. For both nanocarriers, the use of a higher polymer or lipid concentration determines a size increase. For the liposomes, a marked size increase is observed also moving from Z to C chip while in the NPs preparation an increase of the FRR produces much smaller particles. Interestingly, for each nanocarrier all the significant parameters possess an effect of comparable magnitude, determining a size variation with respect to average value of around 7% for liposomes and 24% for NPs. Finally, during the NPs preparation, a significant effect is also due to the interaction between concentration and FRR (upper right panel in figure 7). Specifically, the effect of the increase of concentration is much more relevant when a lower FRR (greater volume of the water phase) is applied. Regarding the PDI of nanoparticles, the effect of concentration and FRR (Supplementary figure 3) is quantitatively equivalent to that observed for the NPs size, a result in agreement with the strong positive correlation previously identified (Supplementary figure 2).

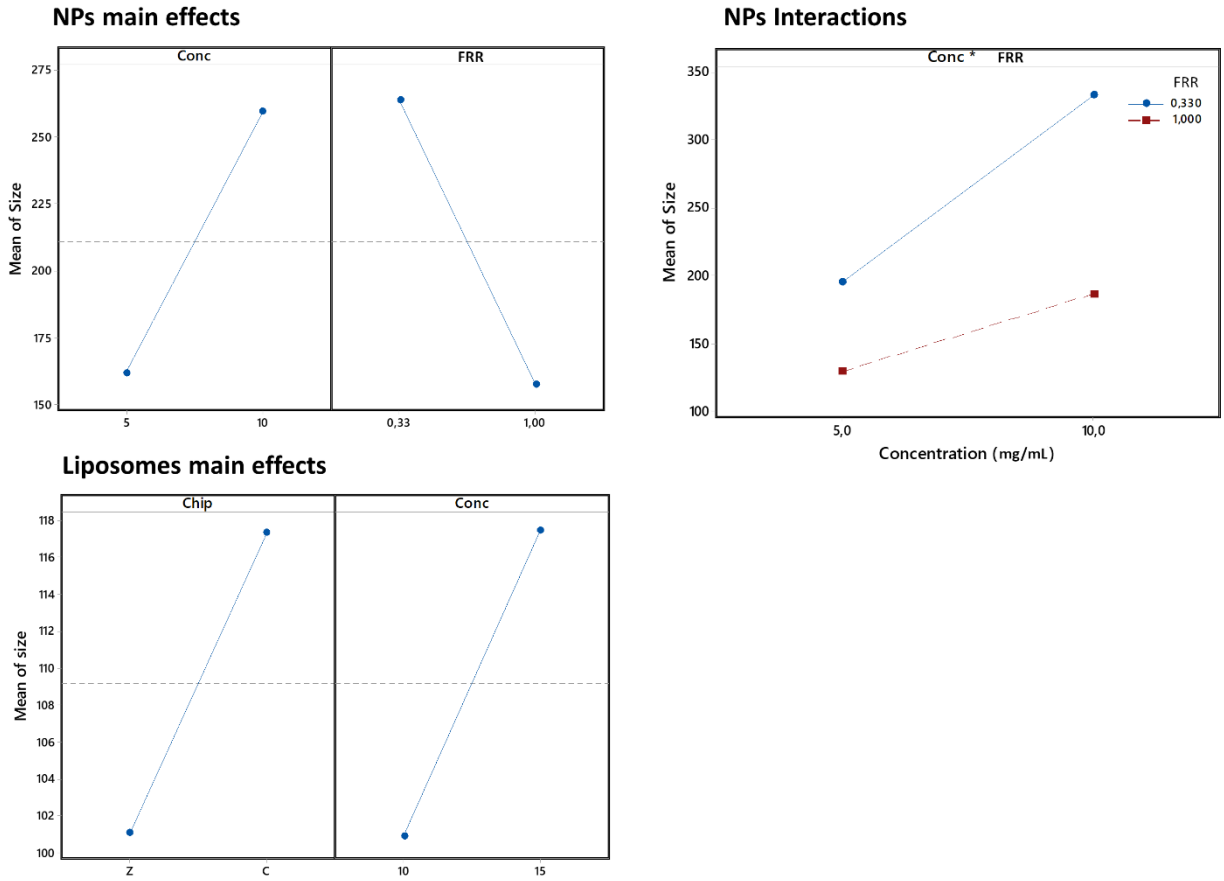

Figure 7. Main effect plots for the size of the NPs (Upper left panel) and liposomes (lower left panel), and interaction plot for the size of the NPs (upper right panel).

These DoE results are important to evaluate how the production parameters influence the final formulation manufactured with the 3D printed microfluidic chip. As usual, each formulation needs

to be optimized with specific parameters since it is impossible to obtain a universal set of values that are efficient for every nanosystem.

3.3 Effect of CBD encapsulation on nanocarriers manufacturing

The DoE allowed understanding how the different experimental parameters affect the unloaded nanocarriers' size and size distributions as a function of the chip design. The next step is to evaluate the eventual effect of an encapsulated drug. As a model drug, we selected CBD, an hydrophobic active molecule with a growing interest in the pharmaceutical field with different applications in a large number of diseases such as dermatological problems, cancer, psychiatric disorders, microbiological infections, and other (Ayati et al., 2020; Karas et al., 2020; Klein, 2005; Sheriff et al., 2020). Since CBD is hydrophobic, its encapsulation into nanocarrier is useful to increase its solubility in water for water-based topical formulations such as hydrogels. The CBD was encapsulated in NPs and liposomes using both chips at the experimental conditions giving the highest and lowest size according to the results of DoE analysis. Such experimental conditions were obtained using the linear partial desirability functions that maximize and minimize the response (size) (Lewis et al., 1998; Vera Candioti et al., 2014) and are reported in the supplementary material (Supplementary table 1).

The comparison between size and PDI (DLS size distribution plots in supplementary figure 4) for unloaded and CBD-loaded nanocarriers is reported in figure 8. The presence of the CBD has a marginal or null effect on the features of NPs and liposomes, which therefore still depend on the experimental preparations parameters as identified with the factorial design analysis.

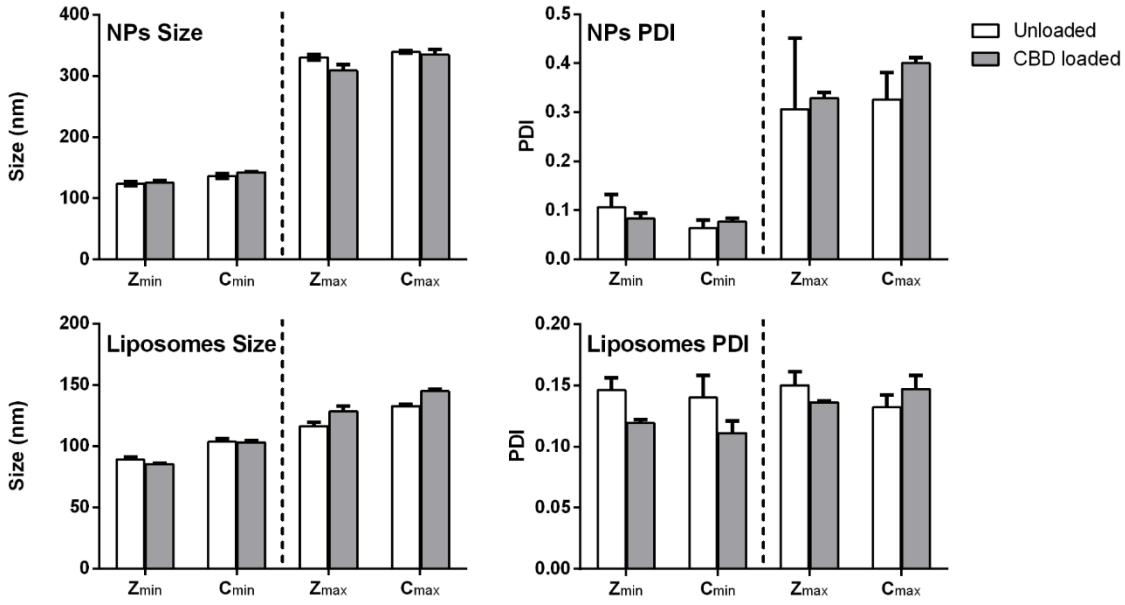

Figure 8. Comparison between the Size and PDI of unloaded and CBD-loaded NPs and liposomes. The x-axis reports the experimental conditions applied where Z and C refer to the chip design and the subscript max or min to the combination of parameters concentration, TFR, and FRR that maximize or minimize the size (the numerical values in supplementary table 1).

Moreover, we evaluated the morphology of the four smallest manufactured loaded nanocarriers using atomic force microscopy (Figure 9). The figure shows the 3D topographic images of: A) CBD loaded PLGA NPs produced with Z chip; B) CBD loaded PLGA NPs produced with C chip; C) CBD loaded liposomes produced with Z chip; D) CBD loaded liposomes produced with C chip. All the observed nanocarriers had spherical structure with well defined regular edges and smooth surface. The average size varied between 80 and 160 nm corroborating the DLS results. It is important to note that the sample scanning area in AFM analysis is very small and not representative.

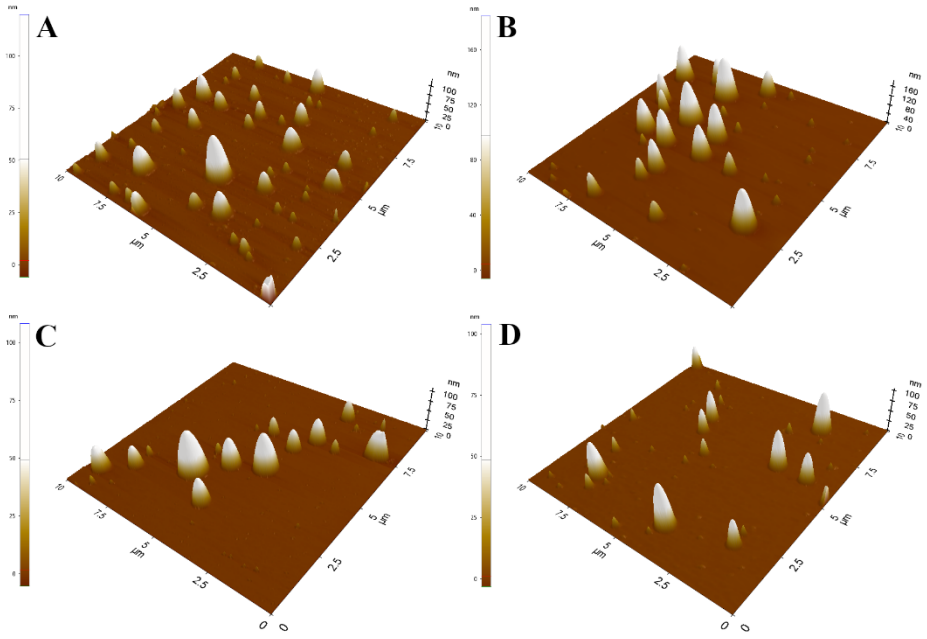

Figure 9. 3D images by AFM of: A) CBD loaded PLGA NPs produced with Z chip; B) CBD loaded PLGA NPs produced with C chip; C) CBD loaded liposomes produced with Z chip; D) CBD loaded liposomes produced with C chip.

Thermal studies were performed to evaluate the interaction between the excipients and the active (Figure 10 and supplementary figure 5). The DSC of unloaded liposomes shows the presence of two endothermic transitions at around 24 and 39 °C, which could be attributed to dimyristoylphosphatidylcholine (DMPC) and dipalmitoylphosphatidylcholine (DPPC) phase transitions in the bilayer (Phospholipon 90-G contains up to 94% of phosphatidylcholines). However, when liposomes were loaded with CBD, the DSC traces showed the disappearance of the peak at 39 °C while the transition of the CBD melting was markedly enlarged. The effect of CBD on DPPC

transition has been previously reported by Bach et al (Bach et al., 1976) and attributed to the limited solubility of cannabinoids in DPPC. Such a results suggest an interaction between CBD and phosphatidylcholine, indicating that CBD is located in the bilayer, or more likely, is partially bond to the bilayer.

For PLGA nanoparticles the DSC highlight a different behaviour. The CBD do not affect the glass transition of the polymer at around 45 °C, however the CBD melting peak is very small and slightly shifted at higher temperature. These results suggested as the drug is mainly encapsulated in an amorphous form stabilized by the polymer.

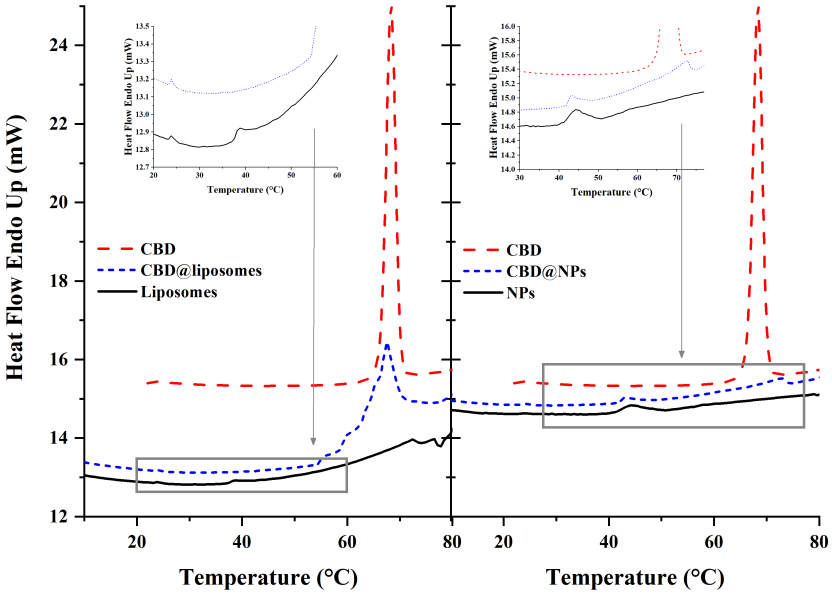

Figure 10. DSC thermograms of pure CBD, liposomes and CBD loaded liposomes (CBD@liposomes) in the left panel with a magnification on lipid transitions. In the right panel, DSC thermograms of CBD, PLGA NPs and CBD loaded PLGA NPs (CBD@NPs) with a magnification on polymer transition.

For the loaded nanocarriers, it has been also determined the encapsulation performance of CBD. As the total added amount of CBD was 3% w/w on excipient weight, it was selected the loading degree (LD%) as the most suitable parameter for evaluating encapsulation, since it is independent from the amount of drug added in each formulation. For each prepared nanocarrier, the LD% can range from 0 (no CBD encapsulated) to 3 (all the added CBD is encapsulated). The results of the LD% (Figure 11) highlight a different behavior between NPs and liposomes. While for the lipid carriers the LD% appears almost independent of the preparation conditions, for NPs the LD% is strongly affected by them and particularly it seems correlated with the size of the particles. The LD results within each type of nanocarriers were further tested using one-way Anova followed by Tukey test. The results of this type of analysis indicated as there were no statistically differences for the LD% for all liposomes

batches. Interestingly, the LD% of NPs showed a variation statistically significant only as a function of the experimental conditions used (max or min) but not as a function of the chip design (Z or C).

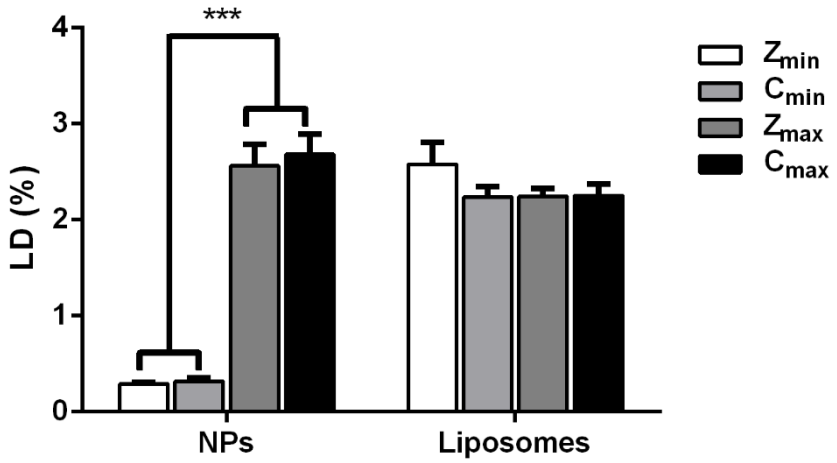

Figure 11. LD% for all the CBD-loaded NPs and Liposomes. The asterisks refer to the the p-value calculated during the post hoc pairwise comparison (Tukey test): * $0.05 < p < 0.01$; ** $0.01 < p < 0.001$; *** $p < 0.001$. The absence of asterisks means a $p > 0.05$.

4. CONCLUSIONS

In this work, simple, easily manufactured 3D printed microfluidic devices have been evaluated. The two developed chips resulted effective to produce model polymeric and lipidic nanocarriers. Thanks to additive manufacturing technology, microfluidics became more accessible to researchers around the world. Our two microfluidic chips STL files are available as supplementary material to be readily printed and used. This has the potential to widen accessibility further by eliminating the design barrier in addition to the fabrication barrier largely limiting access to microfluidic technology at present. Every formulation that takes advantage of microfluidic manufacturing needs to be developed with appropriate microfluidic parameters to reach the desired physicochemical characteristics, and the most influent parameters can be evaluated by DoE as done in this work.

To the best of the author's knowledge, 3D printed PP based microfluidic devices have not previously been realized by FDM printing for the manufacturing of nanocarriers. This is a first approach to this opportunity that can lead to further designs to improve the characteristics of the microfluidic system. The compromise between resolution and material choice will certainly continue to define the preference for either technology.

ACKNOWLEDGMENTS

524 The authors acknowledge Fabio de Belvis for the design of the graphical abstract and Idrofoglia s.r.l.
525 and Techfem S.p.A. for their support to the chip design and computational fluid studies. Moreover,
526 we acknowledge Dr. Michele Menotta (Department of biomolecular sciences, University of Urbino
527 Carlo Bo, Urbino, Italy) for his support with AFM studies.
528
529 **Funding:** This research received no external funding.
530
531 **Conflicts of interest:** The authors declare no conflict of interest
532

REFERENCES

Ansari, M.A., Kim, K.Y., 2010. Mixing performance of unbalanced split and recombine micromixers with circular and rhombic sub-channels. Chem. Eng. J. 162, 760–767. https://doi.org/10.1016/j.cej.2010.05.068

Antoy, J., 2014. A Systematic Methodology for Design of Experiments, in: Design of Experiments for Engineers and Scientists: Second Edition. Elsevier Ltd, pp. 33–50. https://doi.org/10.1016/C2012-0-03558-2

Ayati, Z., Sarris, J., Chang, D., Emami, S.A., Rahimi, R., 2020. Herbal medicines and phytochemicals for obsessive–compulsive disorder. Phyther. Res. https://doi.org/10.1002/ptr.6656

Bach, D., Raz, A., Goldman, R., 1976. The effect of hashish compounds on phospholipid phase transition. BBA - Biomembr. 436, 889–894. https://doi.org/10.1016/0005-2736(76)90420-X

Capretto, L., Cheng, W., Hill, M., Zhang, X., 2011. Micromixing within microfluidic devices. Top. Curr. Chem. 304, 27–68. https://doi.org/10.1007/128_2011_150

Daw, R., Finkelstein, J., 2006. Lab on a chip. Nature. https://doi.org/10.1038/442367a

Desir, P., Chen, T.Y., Bracconi, M., Saha, B., Maestri, M., Vlachos, D.G., 2020. Experiments and computations of microfluidic liquid-liquid flow patterns. React. Chem. Eng. 5, 39–50. https://doi.org/10.1039/c9re00332k

Gueyffier, D., Li, J., Nadim, A., Scardovelli, R., Zaleski, S., 1999. Volume-of-Fluid Interface Tracking with Smoothed Surface Stress Methods for Three-Dimensional Flows. J. Comput. Phys. 152, 423–456. https://doi.org/10.1006/jcph.1998.6168

Heidt, B., Rogosic, R., Bonni, S., Passariello-Jansen, J., Dimech, D., Lowdon, J.W., Arreguin-Campos, R., Steen Redeker, E., Eersels, K., Diliën, H., van Grinsven, B., Cleij, T.J., 2020. The Liberalization of Microfluidics: Form 2 Benchtop 3D Printing as an Affordable Alternative to Established Manufacturing Methods. Phys. status solidi 217, 1900935. https://doi.org/10.1002/pssa.201900935

Hessel, V., Löwe, H., Schönfeld, F., 2005. Micromixers - A review on passive and active mixing principles, in: Chemical Engineering Science. pp. 2479–2501. https://doi.org/10.1016/j.ces.2004.11.033

Hirt, C.W., Nichols, B.D., 1981. Volume of fluid (VOF) method for the dynamics of free boundaries. J. Comput. Phys. 39, 201–225. https://doi.org/10.1016/0021-9991(81)90145-5

Karas, J.A., Wong, L.J.M., Paulin, O.K.A., Mazeh, A.C., Hussein, M.H., Li, J., Velkov, T., 2020. The antimicrobial activity of cannabinoids. Antibiotics. https://doi.org/10.3390/antibiotics9070406

Klein, T.W., 2005. Cannabinoid-based drugs as anti-inflammatory therapeutics. Nat. Rev. Immunol. https://doi.org/10.1038/nri1602

Lee, C.Y., Wang, W.T., Liu, C.C., Fu, L.M., 2016. Passive mixers in microfluidic systems: A review. Chem. Eng. J. https://doi.org/10.1016/j.cej.2015.10.122

Lewis, G.A., Mathieu, D., Phan-Tan-Luu, R., 1998. Pharmaceutical Experimental Design, Pharmaceutical Experimental Design. CRC Press. https://doi.org/10.1201/9780203508688

Liu, Z., Fontana, F., Python, A., Hirvonen, J.T., Santos, H.A., 2019. Microfluidics for Production of Particles: Mechanism, Methodology, and Applications. Small. https://doi.org/10.1002/smll.201904673

Martins, J.P., Torrieri, G., Santos, H.A., 2018. The importance of microfluidics for the preparation of nanoparticles as advanced drug delivery systems. Expert Opin. Drug Deliv. https://doi.org/10.1080/17425247.2018.1446936

Melocchi, A., Uboldi, M., Cerea, M., Foppoli, A., Maroni, A., Moutaharrik, S., Palugan, L., Zema, L., Gazzaniga, A., 2020. A Graphical Review on the Escalation of Fused Deposition Modeling (FDM) 3D Printing in the Pharmaceutical Field. J. Pharm. Sci. https://doi.org/10.1016/j.xphs.2020.07.011

Mer, V.K. La, 1952. Nucleation in Phase Transitions. Ind. Eng. Chem. 44, 1270–1277.

https://doi.org/10.1021/ie50510a027
Metselaar, J.M., Lammers, T., 2020. Challenges in nanomedicine clinical translation. Drug Deliv. Transl. Res. 10, 721–725. https://doi.org/10.1007/s13346-020-00740-5
Morgan, A.J.L., Hidalgo San Jose, L., Jamieson, W.D., Wymant, J.M., Song, B., Stephens, P., Barrow, D.A., Castell, O.K., 2016. Simple and Versatile 3D Printed Microfluidics Using Fused Filament Fabrication. PLoS One 11, e0152023. https://doi.org/10.1371/journal.pone.0152023
Pagano, S., Coniglio, M., Valenti, C., Federici, M.I., Lombardo, G., Cianetti, S., Marinucci, L., 2020. Biological effects of Cannabidiol on normal human healthy cell populations: Systematic review of the literature. Biomed. Pharmacother. https://doi.org/10.1016/j.biopha.2020.110728
Pranzo, D., Larizza, P., Filippini, D., Percoco, G., 2018. Extrusion-Based 3D Printing of Microfluidic Devices for Chemical and Biomedical Applications: A Topical Review. Micromachines 9, 374. https://doi.org/10.3390/mi9080374
Price, A.J.N., Capel, A.J., Lee, R.J., Pradel, P., Christie, S.D.R., 2020. An open source toolkit for 3D printed fluidics. J. Flow Chem. 1–15. https://doi.org/10.1007/s41981-020-00117-2
Romanov, V., Samuel, R., Chaharlang, M., Jafek, A.R., Frost, A., Gale, B.K., 2018. FDM 3D Printing of High-Pressure, Heat-Resistant, Transparent Microfluidic Devices. Anal. Chem. 90, 10450–10456. https://doi.org/10.1021/acs.analchem.8b02356
Sheriff, T., Lin, M.J., Dubin, D., Khorasani, H., 2020. The potential role of cannabinoids in dermatology. J. Dermatolog. Treat. https://doi.org/10.1080/09546634.2019.1675854
Tothill, A.M., Partridge, M., James, S.W., Tatam, R.P., 2017. Fabrication and optimisation of a fused filament 3D-printed microfluidic platform. J. Micromechanics Microengineering 27, 035018. https://doi.org/10.1088/1361-6439/aa5ae3
Trotta, M., Peira, E., Debernardi, F., Gallarate, M., 2002. Elastic liposomes for skin delivery of dipotassium glycyrrhizinate. Int. J. Pharm. 241, 319–327. https://doi.org/10.1016/S0378-5173(02)00266-1
Valencia, P.M., Farokhzad, O.C., Karnik, R., Langer, R., 2012. Microfluidic technologies for accelerating the clinical translation of nanoparticles. Nat. Nanotechnol. 7, 623–629. https://doi.org/10.1038/nnano.2012.168
Vasilescu, S.A., Bazaz, S.R., Jin, D., Shimoni, O., Warkiani, M.E., 2020. 3D printing enables the rapid prototyping of modular microfluidic devices for particle conjugation. Appl. Mater. Today 20, 100726. https://doi.org/10.1016/j.apmt.2020.100726
Vera Candioti, L., De Zan, M.M., Cámara, M.S., Goicoechea, H.C., 2014. Experimental design and multiple response optimization. Using the desirability function in analytical methods development. Talanta. https://doi.org/10.1016/j.talanta.2014.01.034
Waheed, S., Cabot, J.M., Macdonald, N.P., Lewis, T., Guijt, R.M., Paull, B., Breadmore, M.C., 2016. 3D printed microfluidic devices: Enablers and barriers. Lab Chip 16, 1993–2013. https://doi.org/10.1039/c6lc00284f
Weller, H.G., Tabor, G., Jasak, H., Fureby, C., 1998. A tensorial approach to computational continuum mechanics using object-oriented techniques. Comput. Phys. 12, 620. https://doi.org/10.1063/1.168744
Wu, Q., Liu, J., Wang, X., Feng, L., Wu, J., Zhu, X., Wen, W., Gong, X., 2020. Organ-on-a-chip: Recent breakthroughs and future prospects. Biomed. Eng. Online. https://doi.org/10.1186/s12938-020-0752-0
Zhao, X., Bian, F., Sun, L., Cai, L., Li, L., Zhao, Y., 2020. Microfluidic Generation of Nanomaterials for Biomedical Applications. Small 16, 1901943. https://doi.org/10.1002/smll.201901943